Hindawi
Geofluids
Volume 2022, Article ID 2012776, 13 pages
https://doi.org/10.1155/2022/2012776

Research Article

Creep Properties of Mudstone Interlayer in Bedded Salt Rock Energy Storage Based on Multistage Creep Test: A Case Study of Huai'an Salt Mine, Jiangsu Province

Jie Chen,[1,2] He Chen,[1,2] Fei Wu ,[1,2] Deyi Jiang,[1,2] Hao Zhang,[1,2] Renbo Gao,[1,2] and Bowen Ding[1,2]

[1]*State Key Laboratory of Coal Mine Disaster Dynamics and Control, Chongqing University, Chongqing 400044, China*
[2]*School of Resources and Safety Engineering, Chongqing University, Chongqing 400044, China*

Correspondence should be addressed to Fei Wu; wufei3616@cqu.edu.cn

Received 30 April 2022; Accepted 11 July 2022; Published 29 August 2022

Academic Editor: Guang-Liang Feng

Salt rock is internationally recognized as an excellent medium for energy storage. However, most of the domestic salt mines are lacustrine laminated formations with mudstone interlayers, which have different creep characteristics to pure salt rocks. Therefore, in this paper, uniaxial compression creep tests were carried out on a mudstone interlayer in Huai'an, Jiangsu, China, and the multistage creep mechanical behavior of the mudstone interlayer was investigated using acoustic emission (AE) technology. The results show that at low stress levels, the axial deformation of the interlayer is greater than the lateral deformation. As the increase of the stress level, the lateral deformation becomes more significant, and the corresponding axial and lateral steady-state creep rates both exhibit nonlinear acceleration with the increase of the loading stress. In the initial loading stage of each stress level, the mudstone interlayer releases a large number of AE signals. After the creep stabilization, the AE signals decreased obviously, and a large number of AE signals were released at the last stress level. Based on the creep test data, an improved fractional viscoelastic-plastic model was fitted to it and compared with the Nishihara model. The applicability of the model was also tested, and the model was found to be a good description of the mudstone interlayer after oil erosion. The research results reflected the creep law of the mudstone interlayer to a certain extent and are expected to serve as a reference to studies on the long-term stability of the surrounding rock of a bedded salt rock energy storage.

1. Introduction

As the lifeblood of the country, a crisis in energy would have an adverse impact on the country's economic security and social stability [1, 2]. With the gradual transformation of global energy sources, renewable energy sources such as photovoltaic power generation and wind power generation are gaining more and more attention in the world [3, 4]. Because salt rock has good creep performance and can meet the long-term and frequent injection and production demand of energy storage, salt cavern is often used as the best place for compressed gas energy storage technology [5–7]. A sketch map of the salt cavern compressed air energy storage is shown in Figure 1. However, salt deposits in China are mostly lakeside sedimentary structures, which are characterized by a large mudstone interlayer content and a thin single layer thickness [8, 9]. The existence of many mudstone interlayers makes the physical and mechanical properties of salt mines more complex, especially under high working pressure, and the creep mechanical properties of interlayer and salt rock are different [9]. The creep characteristics of salt rock is one of the core issues in the long-term stability research of surrounding rock with salt cavern energy storage, and it is also an important factor affecting the long-term operation of underground deep energy storage.

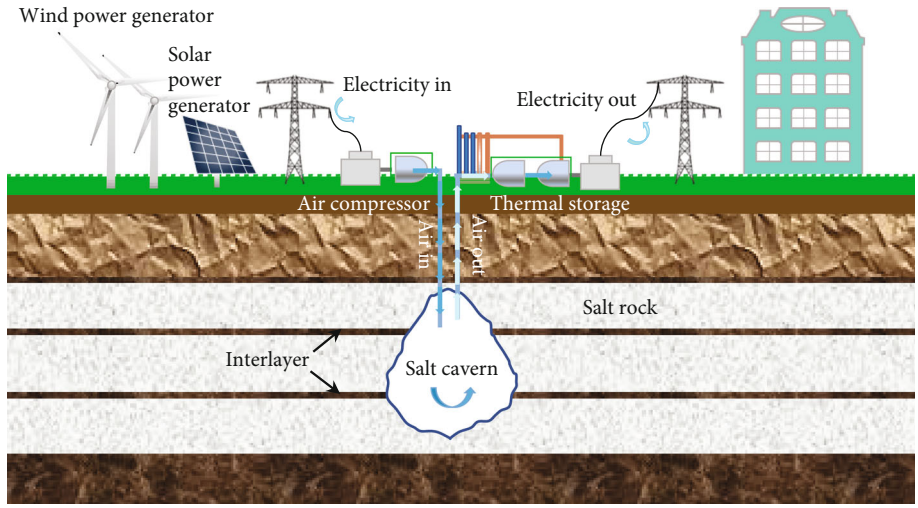

Figure 1: Sketch of salt cavern compressed air energy storage.

In recent years, many scholars have focused on the salt rock creep characteristics of the surrounding rock of the salt cavern energy storage. Liang et al. [10] conducted experimental research and theoretical analysis on the creep of salt rock and established the coupled constitutive equation of transient creep and steady-state creep of salt rock. The interlayer in the salt rock is also an important factor affecting the stability of the surrounding rock of the reservoir. The creep characteristics of the layered salt rock are mainly derived from the salt rock part, in which the interlayer has a good inhibitory effect on the creep deformation of the salt rock [11]. The mechanical properties of the interface between the salt rock and the interlayer are between the salt rock and the interlayer, and it is not a weak zone [12]. Ślizowski and Lankof [13] studied the rheological properties of the mudstone interlayer in the bedded salt rock and believed that the mudstone interlayer with higher rock salt content is a good medium for nuclear waste storage. Li and Yang [14] proposed a three-dimensional extended Cosserat medium constitutive model of layered rock salt and used it for the stability analysis of underground salt caverns. Zhou et al. [15] established a fractional order model of salt rock, which can provide a certain reference for the failure judgment of salt cavern. Yang et al. [16] proposed a three-dimensional geomechanical model to evaluate the feasibility of using UGS layered rock salt caverns and verified its accuracy through on-site sonar measurement on-site data. Tang et al. [17] conducted creep experiments on salt rock mudstone and salt rock with muddy interlayer under triaxial conditions, respectively, and studied the relationship between the duration of initial creep stage and stable creep rate of the three rock samples.

Although there are many studies on the creep characteristics of salt rock, there are relatively few studies on the creep characteristics of interlayer in bedded salt rocks in China, especially in determining the creep parameters of mudstone interlayer. Therefore, understanding the creep mechanical behavior of mudstone interlayers is a prerequisite for the design of operating conditions during the operation of the salt cavern oil storage.

In this paper, uniaxial compression multistage creep tests were carried out on mudstone interlayer samples in the salt mining area of Huai'an, Jiangsu Province, and the creep properties of the mudstone interlayer were analyzed using acoustic emission techniques. Based on the experimental results, a modified viscoelastic-plastic damage creep model based on fractional order derivatives was used to verify the evolution of creep curves under graded loading conditions, and the applicability of the model was discussed and verified.

2. Experimental Scheme

2.1. Sample Preparation. The samples were taken from the mudstone interlayer in Huai'an Salt Mine area, Jiangsu Province, and the sampling depth was about 1000 m, which was a typical calcareous mudstone interlayer. As the sample belongs to the mudstone interlayer in bedded salt rock, the core contains some clay minerals and soluble salts. The location of sample is shown in Figure 2. Ordinary water-soluble drilling or dry lathe machining will cause great damage to the rock. Therefore, the samples were wire-cutting cut by SM 150 sample manufacturer equipment. This preparation method does little damage to the rock sample. The samples is processed into cylindrical sample with a diameter of about 50 mm and a height of 100 mm, and the accuracy was controlled within 0.2 mm. All samples met the requirements of industry standards (GB/T50266, 2013; SL264, 2001).

2.2. Test Method and Process. The test equipment adopts the salt rock mechanics tester independently developed by the State Key Laboratory of Coal Mine Disaster Dynamics and Control of Chongqing University. Before the test, the average uniaxial compressive strength of the mudstone interlayer was obtained through the basic mechanical test, and the obtained uniaxial compressive strength was used as a reference for the selection of loading stress in the creep test. The test adopts the uniaxial grading loading method, the load is applied step by step from small to large, and each stage of loading lasts for about 24 hours until the sample is

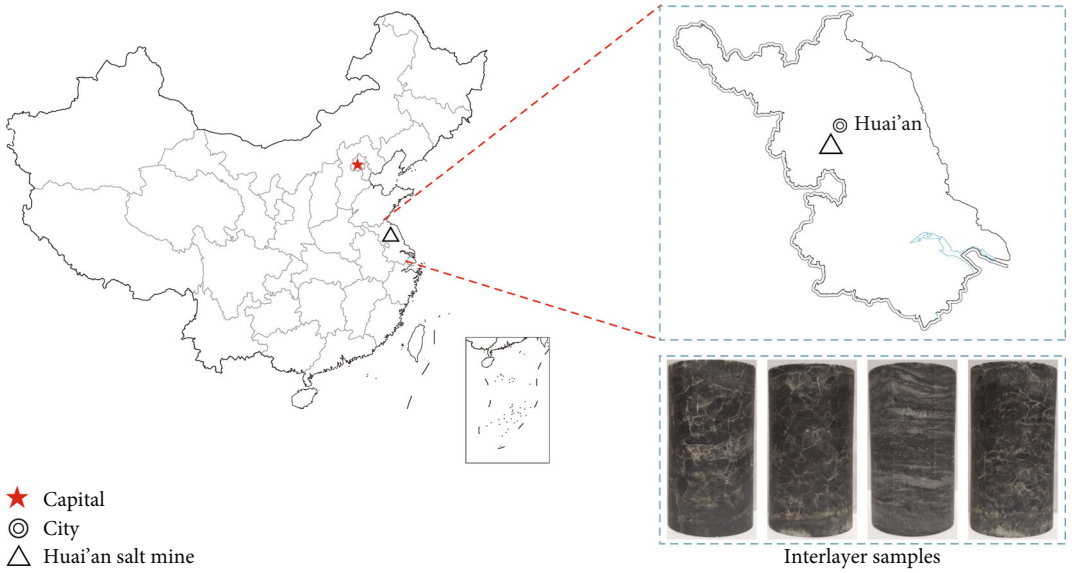

Figure 2: Location of the sample collection.

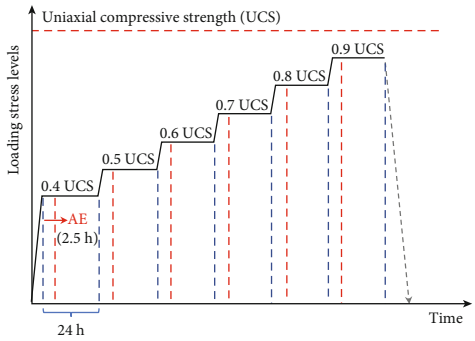

Figure 3: The loading paths of the creep test.

completely destroyed. Within 2.5 hours after the loading all stress levels, acoustic emission (AE) was used to monitor the damage characteristics of the rock from initial loading to steady creep. The loading path of the creep test is shown in Figure 3.

The ratio of the predetermined loading stress to the uniaxial compressive strength (UCS) is defined as loading ratio indicator (k), which is expressed as [18]

$$k = \frac{\sigma_a}{\sigma_{\text{ucs}}}, \tag{1}$$

where σ_a is the predefined loading stress, and σ_{ucs} is the uniaxial compressive strength. Table 1 lists the loading ratios and corresponding loading stresses of the samples.

3. Results and Analysis

3.1. Creep Strain Analysis. According to the difference of strain rates, the creep process can be divided into three stages: the transient creep stage (strain rate keeps decreasing with time), the steady creep stage (strain rate remains constant, also known as the steady-state creep stage), and the accelerated creep stage (strain rate increases rapidly until failure), as shown in Figure 4. ε_0, ε_c, and ε_t are the instantaneous strain (i.e., initial strain), creep strain, and total strain at each stress level, respectively. i.e., $\varepsilon_t = \varepsilon_0 + \varepsilon_c$.

Figure 5 shows the uniaxial compression creep test curves of mudstone interlayers under different stress levels. From the creep test curve, it can be seen that at the moment of loading at each stress level, the sample has a remarkable transient elastic response, and then creep deformation increases with time. In the first three creep stages, the sample showed obvious initial creep stage and steady-state creep stage. At the initial stage of loading at each level of stress, the axial strain increases with time, while the axial creep strain rate decreases with time. After a certain period of time, the creep rate gradually tends to be stable, entering a relatively stable creep stage. In the fourth creep stage, the creep deformation obviously has three creep stages. After the steady creep stage of rock, the strain rate of the sample increases rapidly and enters the obvious nonlinear accelerated creep stage, which shows the characteristics of accelerated creep until the failure of the sample. Compared with axial strain, the transverse strain of the sample presents the same changing trend.

The creep strains of the samples under various loading stress levels were quantitatively analyzed. Figure 6 shows the creep isochronous strain curves of the samples loaded for 24 h under axial loading stresses of 10.24 MPa, 12.79 MPa, 15.34 MPa, and 17.89 MPa, respectively.

It can be seen from Figure 6 that the creep strain of the specimen increases with the increase of the loading ratio, and both of them show a high degree of nonlinearity. When the loading ratio reaches 0.6, the whole creep isochronous strain curve increases nonlinearly with the increase of stress. By fitting the experimental data, it is found that the relationship between the creep strain and the loading ratio of the

Table 1: Loading ratios (k) and the corresponding loading stresses (σ_a).

k	Sample	0.4	0.5	0.6	0.7	0.8	0.9
σ_a (MPa)	Mudstone interlayer	10.24	12.79	15.34	17.89	20.44	22.99

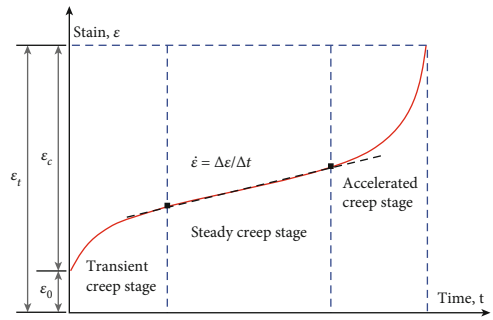

Figure 4: Typical creep curve of rock material.

sample can be described by an exponential function, and the fitting coefficient is good. The specific fitting data is shown in Figure 6. As the loading stress increases, the curve exhibits a nonlinear growth characteristic, which is related to the initiation and accumulation of damage inside the rock. However, the lateral creep change of the sample becomes more and more obvious, which is much larger than the axial creep. As the stress level increases, the creep rate and creep deformation of the sample differ. The larger the axial stress, the faster the creep rate and the larger the corresponding creep deformation. It can be seen that the lateral creep of the mudstone interlayer in the salt cavern energy storage is more sensitive than the axial creep.

3.2. Steady-State Creep Strain Rate Analysis. Figure 7 shows the steady-state creep rates of samples under different stress levels. According to previous experimental study of salt rock creep under the condition of graded loading [10], the steady-state creep rate of rock has nothing to do with the loading history. Therefore, applying multistage creep test loading to the same sample can not only avoid the influence of sample dispersion on the test results but also analyze the change of the steady-state creep rate of the rock under different stress levels. As shown in Figure 7, as the loading stress increases, the steady-state creep rate of the mudstone interlayer shows an upward trend, and the two show a high degree of nonlinearity. Analysis of the data in the figure shows that this relationship can be basically fitted by Eq. (2).

$$\dot{\varepsilon} A e^{bk} + B = , \tag{2}$$

where $\dot{\varepsilon}$ is the steady-state creep strain rate, k is loading ratio indicator, and A, B, and b are constants related to mudstone interlayers. Table 2 shows the relevant fitting data of mudstone interlayers.

The fitting correlation coefficients of the axial steady creep rate and the lateral steady creep rate are 0.99977 and 0.99992, respectively, indicating that the experimental data can describe the variation characteristics of the steady-state creep rate of the sample well. With the increase of stress level, the creep rate and creep deformation of the sample are different. The greater the axial stress, the faster the creep rate and the larger the corresponding creep deformation. However, the lateral creep rate changes more and more obviously, far greater than the axial steady creep rate. When the stress state is at a high stress level, the lateral creep of the rock is more sensitive than the axial creep.

3.3. The Effect of Stress Level on Instantaneous Strain and Creep Strain. Figure 8 shows the relationship between the instantaneous strain(ε_0) and the stress level (i.e., the loading ratio). It can be seen that as the stress level increases, the axial instantaneous strain of the sample gradually increased. At the same time, the lateral instantaneous strain tends to increase with the increase of the stress level. The difference in the instantaneous strain of the rock at various stress levels is attributed to the change in the damage inside the sample. When the loading ratio increases from 0.6 to 0.7, the instantaneous strains of the sample increase significantly. It can be considered that when the loading ratio is 0.6, the internal structure of the sample has obvious damage, and most of the pores of the sample are compacted. Figure 8(b) shows the relationship between the lateral instantaneous strain (ε_0) and the stress level (ie, the loading ratio). It can be seen from the figure that the axial instantaneous strain of the mudstone interlayer is slightly larger than the lateral instantaneous strain, but the total lateral strain of mudstone interlayer is much larger than the total axial strain. This change in the axial instantaneous strain of the sample shows that with the continuous increase of the stress level, there is obvious damage inside the sample, which causes the axial instantaneous strain to increase significantly. This change in axial instantaneous strain caused by the aggravation of internal damage is far more sensitive than that of the change in lateral instantaneous strain.

Figure 9(a) shows that for the natural sample, the axial creep strain (ε_c) shows an upward trend as the stress level (i.e., the loading ratio) increases. When the loading ratio is 0.7, the axial creep strain is 1.191×10^{-2}, which is about twice the axial creep ($6.603 \times 10 - 3$) when the loading ratio is 0.6. It shows that under the high stress level, more serious damage is accumulated in the creep stage. At this time, when the loading ratio is 0.7, the creep strain increased continuously and entered the accelerated creep stage, where microcracks expanded and grew at an accelerated rate, resulting in a large number of cracks, leading to be final macro failure. Figure 9(b) shows the relationship between the lateral creep strain (ε_c) and the loading ratio. At each stress level, the variation trends of the lateral creep strain and the axial creep strain of the mudstone interlayer are basically the same. It should be noted that the transverse creep strain is much larger than the axial creep strain at each stress levels. When the loading ratio is $0.4 \sim 0.5$, the transverse creep strain of

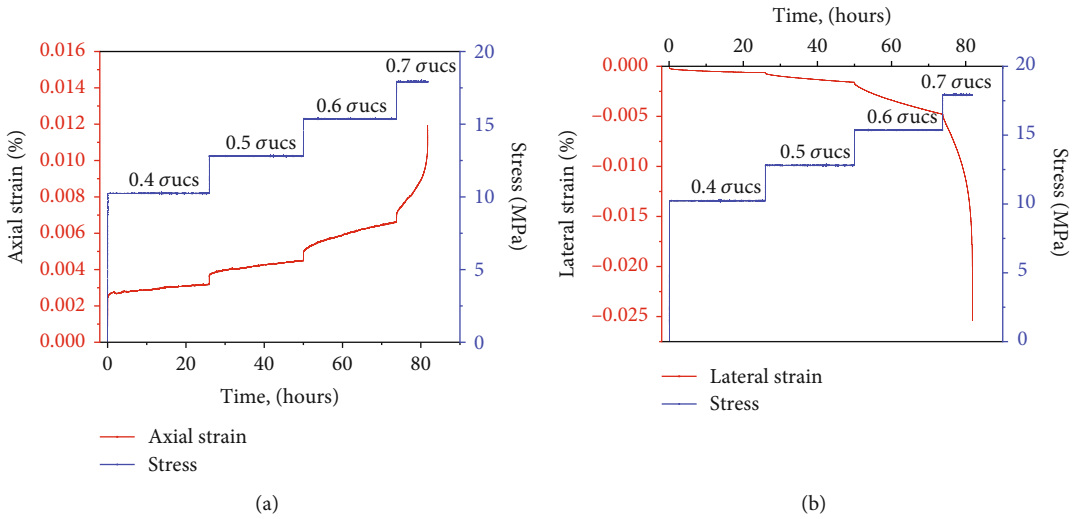

Figure 5: Creep testing curves under different stress levels.

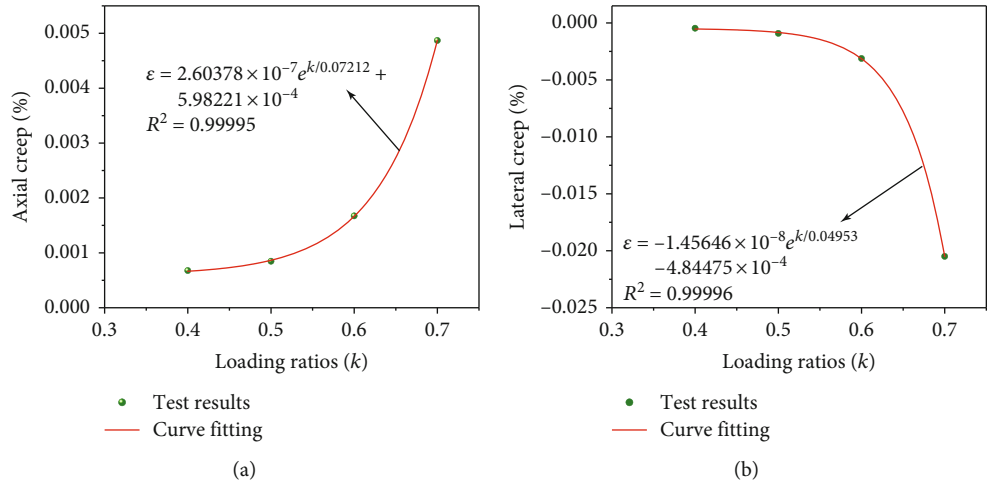

Figure 6: Creep testing curves under different stress levels.

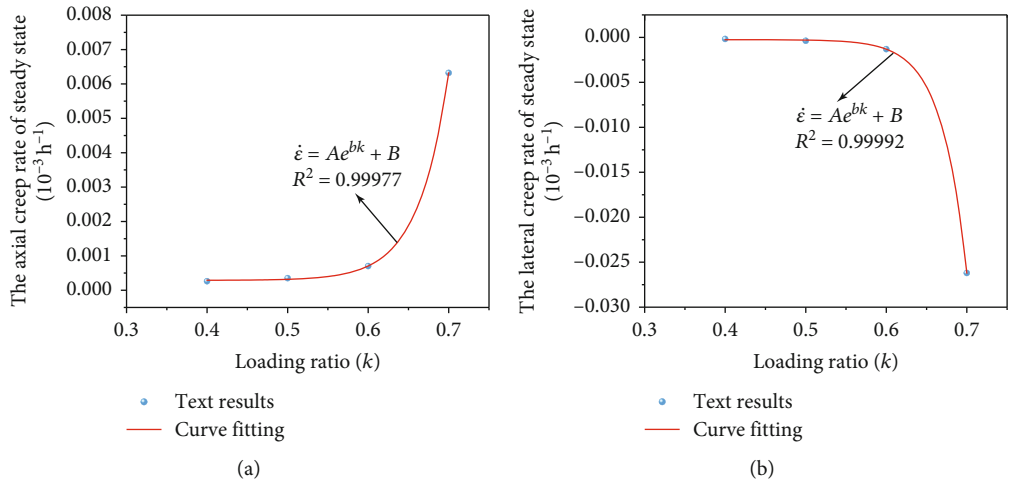

Figure 7: The relationship between steady-state creep rate and loading ratio of the mudstone interlayer.

Table 2: Statistics of fitting parameters of steady-state creep rate (unit: h^{-1}) of the mudstone interlayer.

Index	Parameter A	Parameter B	Parameter b	R^2
Axial creep rate	$4.56416 \times 10 - 12$	$2.89069 \times 10 - 5$	0.03743	0.99977
Lateral creep rate	$-4.96431 \times 10 - 13$	$-2.55305 \times 10 - 5$	0.03128	0.99992

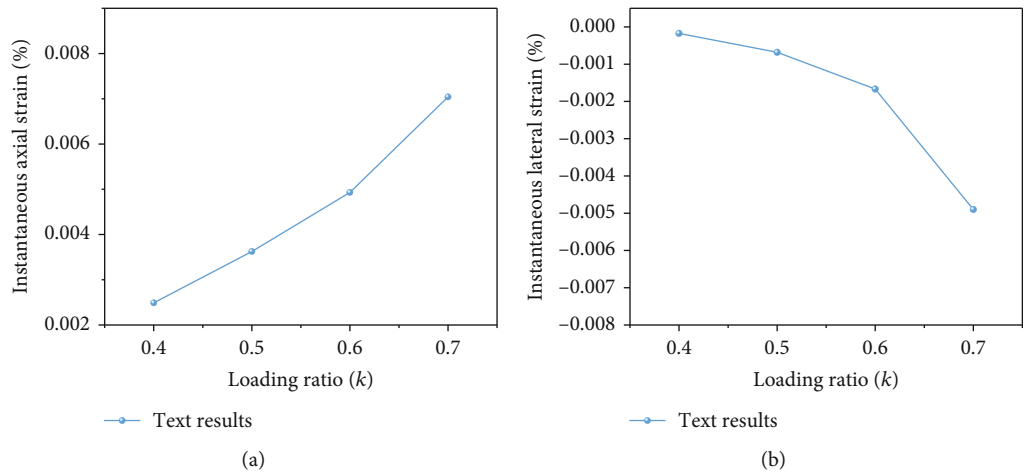

Figure 8: Relationship between the stress level and the instantaneous strain.

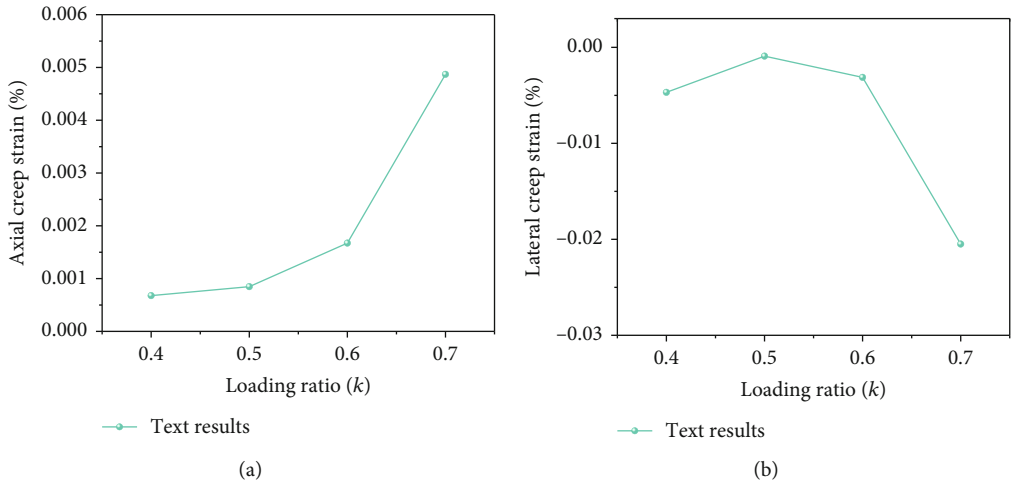

Figure 9: Relationship between the stress level and the creep strain.

the specimen shows a decreasing trend. This may be due to the fact that the initial porosity in the specimen was compacted at the initial stage of loading, resulting in a large lateral deformation. When the loading ratio reaches 0.6, the lateral creep strain is much larger than the axial creep strain with the increase of stress level.

3.4. Determination of Long-Term Strength of Mudstone Interlayer. The long-term strength of rock is an important indicator to measure the long-term stability of rock. At present, the most commonly used method to determine the long-term strength of rock is to use the isochronous stress-strain curve inflection point method and the steady-state creep rate inflection point method [19]. Therefore, several common methods are used in this paper to analyze the long-term strength of mudstone interlayers.

3.4.1. Isochronous Stress-Strain Curve Inflection Point Method. The isochronous stress-strain curve refers to the relationship between the creep deformation and stress corresponding to the same time in a set of creep curves with different stress levels. The stress corresponding to the inflection point of the curve is the long-term strength of the rock [20]. In this paper, isochronous stress-strain curves are plotted separately for samples at each stress level for $t = 24$ hours, based on experimental data, as shown in Figure 10.

As shown in Figure 10, when the axial stress is not greater than 15.34 MPa, the isochronous stress-strain curves

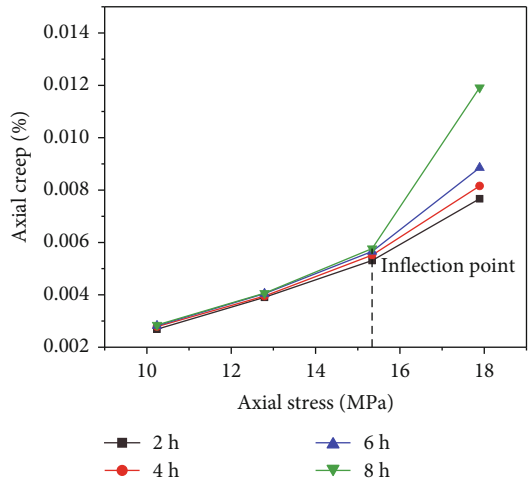

Figure 10: Isochronal stress-strain curves.

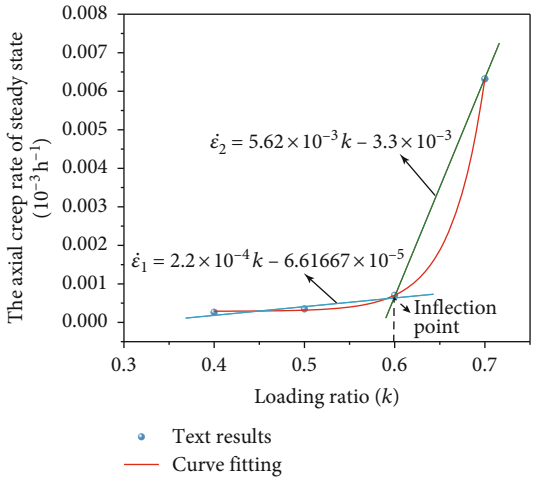

Figure 11: Determination of inflection point of steady creep rate.

at each moment almost coincide. When the axial stress exceeds 15.34 MPa, the curve starts to deflect showing a nonlinear characteristic. It can be seen that when the axial stress is greater than 15.34 MPa, the four isochronous stress-strain curves in the diagram begin to transition from straight to curved there is an obvious inflection point. The long-term strength of the mudstone interlayer can be determined from the isochronous stress-strain curve method by determining the stress value corresponding to the inflection point. That is, the stress value corresponding to the inflection point is $0.6\sigma_{ucs}$.

3.4.2. Inflexion Point Method of Steady Creep Rate. As can be seen from Figure 11, when the axial stress is at a low level, the axial strain rate decreases with time and gradually stabilizes, entering a more steady-state creep phase. As the stress level increases, the steady-state creep rate of the specimen also increases. When the stress level is high, viscoelastic-plastic creep occurs in the mudstone interlayer, and the creep rate of the specimen increases and eventually creep damage occurs. A more accurate method for determining

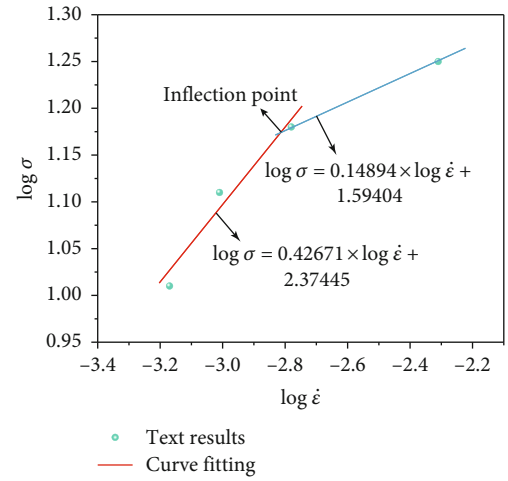

Figure 12: Double logarithmic creep rate inflection point method.

the long-term strength of rocks based on the steady-state creep rate inflection point method [21]. As can be seen in Figure 11, there is an inflection point in the curve as the stress level continues to increase. The rock creep rate increases slightly before the inflection point, and the curve increases abruptly and nonlinearly after the inflection point. The data before and after the inflection point were fitted with two linear functions to obtain two fitted curves:

$$\dot{\varepsilon_1} = 2.2\times10^{-4}k - 6.61667\times10^{-5}, \quad (3)$$

$$\dot{\varepsilon_2} = 5.62\times10^{-3}k - 3.3\times10^{-3}. \quad (4)$$

The loading stress corresponding to the intersection of the two straight lines can be taken as the long-term strength of the rock, which means that the creep rate of the mudstone interlayer increases significantly when the loaded uniaxial stress reaches 15.3 MPa. Thus, the long-term strength of the mudstone interlayer determined by the steady-state creep rate inflection point method is approximately 15.3 MPa, which is not significantly different from the long-term strength of the mudstone interlayer determined by the isochronous stress-strain curve.

3.4.3. Double-Segment Power Function Inflection Point Method. Wu et al. [22] found that the steady-state creep rate was linearly related to the loading stress, and that there was an inflection point where the loading stress was the long-term strength of the rock. This two-segment power function inflection point method is similar to the steady-state creep inflection point method as a new method for determining long-term strength. First, both the loading stress and the steady-state creep rate were taken as logarithms, and then the data were fitted to a segmented linear fit. As both linear functions describe the logarithmic data better, the intersection of the two can be used as the long-term strength of the rock. The experimental data was processed according to this method, and the results are shown in Figure 12. Processing the longitudinal coordinates corresponding to the intersection points gives a

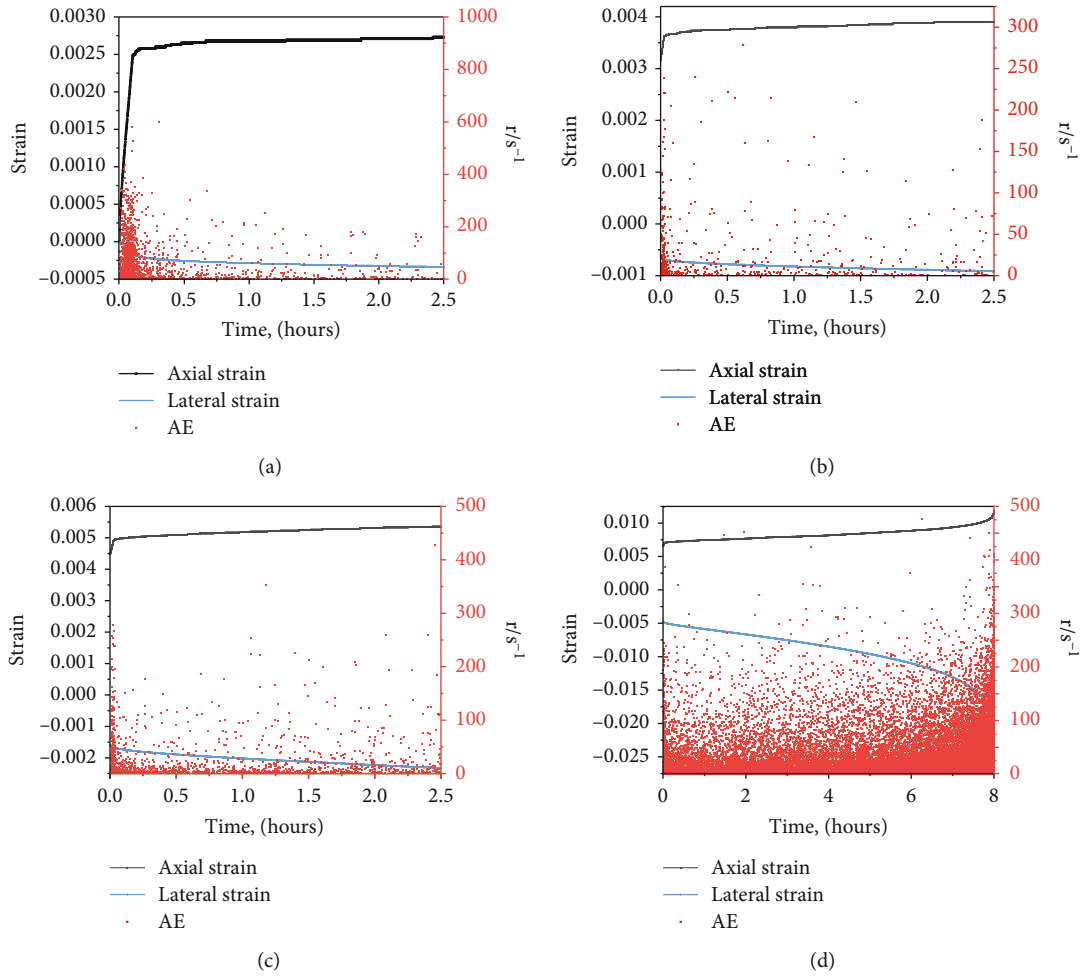

Figure 13: The relationship between the time, strain, and AE signal of the mudstone interlayer at each loading stage.

corresponding stress of 14.97 MPa, i.e., the long-term strength of the mudstone interlayer obtained by this method is approximately 14.97 MPa.

From the above analysis, it can be seen that the long-term strength of the mudstone interlayer in the test ranged from approximately 14.97 to 15.34 MPa. It is easy to see that all three long-term strength determination methods are influenced by creep stress levels and loading times. Therefore, the long-term strengths obtained using several different methods as described above will be more accurate.

3.5. Relationship between Stress Loading Level and AE. After the rock is subjected to external loads, the strain energy stored in the rock is instantly released to generate elastic waves, causing the initiation and expansion of internal cracks and generating AE signals. AE can reflect the evolution process of micro-cracks in rock [23]. Therefore, during the test process, AE technology was used to monitor the damage characteristics of rock during creep. AE was used to monitor the damage characteristics of rocks from initial loading to steady creep under different stress loading levels. Figure 13 shows the relationship between the loading time, strain, and AE signals of mudstone interlayers. It can be seen from the figure that the mudstone interlayer has typical AE characteristics corresponding to it at each loading stage. In the initial loading stage of each stress level, a large number of AE signals are generated, and after the creep stability, the AE signals are obviously reduced, and a large number of AE signals are generated in the whole stage of the last stress level. At the stress loading level of $0.4\sigma_{ucs}$, the AE signals generated by natural samples are obviously more than those of other stress levels (except for the last stress level). This shows that in the initial stage of loading, the initial microcracks or pores inside the sample are gradually squeezed and closed, resulting in impact damage and more acoustic emission signals. This shows that in the initial stage of loading, the initial microcracks or pores inside the sample are gradually squeezed and closed, resulting in impact damage and more AE signals. When the stress level is stable, there is enough time for the elastic strain caused by the imbalance between grains to coordinate and balance with each other; so, there will be no large number of AE signals in the initial stage of loading, only a small number of weak AE signals. However, with the increase of the stress level, the sample is in the elastic deformation stage approximately, the elastic deformation accumulated in an instant will have a

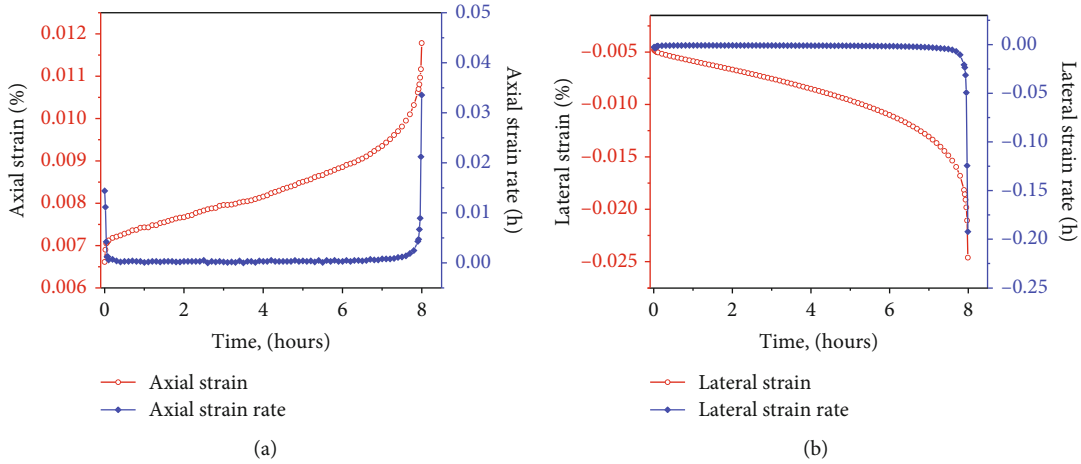

Figure 14: Creep strain and the associated creep strain rate of the mudstone interlayer at the final stress level.

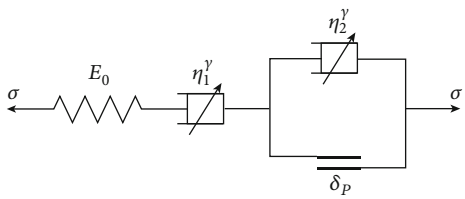

Figure 15: Sketch map of the creep constitutive model.

certain rebound recovery space due to the rapidly generated crack and cavity, and no new crack will be generated [24]. When the stress loading level is at the last level, the internal cracks of the samples develop rapidly, and the internal structure is unstable and destroyed, resulting in a large number of AE signals.

As the captured AE signals is the elastic energy released by the internal microstructure instability [25, 26], the side view of the AE signals reveals the damage caused by the mudstone interlayer inside the samples at various stress levels [27–29].

4. Fractional Viscoelastic-Plastic Creep Model of Mudstone Interlayer

4.1. Creep Strain Analysis of Mudstone Interlayer at Above Yield Stress. As can be seen from Figure 5, when the loading stress is lower than the yield stress, the creep deformation of the mudstone interlayer has two creep phases: the initial creep phase and the steady-state creep phase. And when the loading stress is higher than the yield stress, the creep deformation obviously has three creep stages. When the mudstone interlayer enters the accelerated creep stage, the strain rate of the sample increases rapidly, showing obvious nonlinear accelerated creep characteristics until the sample is damaged.

Figure 14 shows the creep strain of the mudstone interlayer at the final stress level and the related creep strain rate. Different from other stress levels, accelerated creep occurs in both axial and lateral creep at this stress level. It shows all the creep behaviors of the samples at the final stress level. It can be seen from the creep strain rate that there are three creep stages in the creep process of the mudstone interlayer under the creep failure stress level: initial creep stage when the strain rate decreases, the steady-state creep stage at a constant strain rate, and finally, the accelerated creep stage. The creep process duration of the specimen at the last stress level is 8.0 h, while the axial creep and transverse creep reach the accelerated creep stage after experiencing the initial creep stage and steady-state creep stage of about 7.3 h. It can be clearly seen from Figure 15 that the lateral creep rate of the mudstone interlayer in the accelerated creep stage is greater than the axial creep rate, while in the initial creep stage, the lateral creep rate of the mudstone interlayer is smaller than the axial creep rate. It can be seen that the lateral creep rate of the mudstone interlayer is greater than the axial creep rate at the near failure stage.

4.2. Improvement on Fractional Viscoelastic-Plastic Creep Model. Since the rock does not show obvious nonlinear deformation before entering the accelerated creep stage, it can be considered that the damage degree of the rock is small [30, 31]. As the rock does not exhibit significant nonlinear deformation until it enters the accelerated creep phase, the degree of damage to the rock can be assumed to be minimal. Based on the above reasons, this paper attempts to establish and improve the fractional viscoelastic-plastic creep damage model to describe the creep deformation characteristics under the last stress level.

Zhou et al. [32] established a rheological model of salt rock based on fractional derivatives and found that this model could accurately describe the rheological test curve of salt rock. Xu et al. [33] found that the deformation behavior of marble under high confining pressure is similar to that of soft rock, it has the characteristics of ductility and improved on the basis of the fractional derivative salt rock rheological model, and a fractional creep model suitable for marble is established. The mudstone interlayer studied in this paper is taken from the Huai'an salt rock mining area, Jiangsu Province, and contains a certain amount of salt, which not only retains the ductility of soft rock but also has the brittle failure characteristics of hard rock. Therefore,

Table 3: Parameters determined by fitting analysis based on creep test of mudstone interlayer ($\sigma \geq \sigma_s$).

Stress/MPa	E_0/GPa	E_1/GPa	η_1^γ/(GPa·h^γ)	η_2^γ/(GPa·h^γ)	γ	α /h^{-1}	R
Nishihara model	2.59	59.63	5625.47	2318.18	1	0	0.9816
Fractional viscoelastic-plastic model	2.56		4.47	30.68	0.86	0.74	0.9938

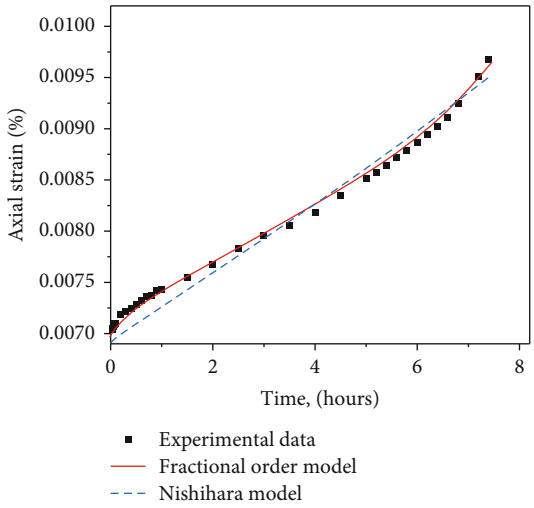

Figure 16: The model fitting data were compared with the experimental data.

the improved fractional creep model is used to investigate the creep characteristics of mudstone interlayers under the action of hierarchical loading stress [34].

For the definition of fractional calculus, please refer to the references [34–36]. The following is a brief introduction to the Abel dashpot. The constitutive relation of the Abel dashpot [32] is

$$\sigma = \frac{\eta d^\gamma \varepsilon(t)}{dt^\gamma (0 \leq \gamma \leq 1)}, \tag{5}$$

where η is the viscosity coefficient, and γ is derivative order.

When $\gamma = 0$, the stress-strain relationship is linear, which satisfies Hooke's law, which is an ideal elastic body. When $\gamma = 1$, the stress-strain relationship is the first derivative, which is a Newtonian fluid. It can be concluded that the properties of Abel dashpot are between elastic body and Newtonian fluid, and its physical meaning can be used to describe the constitutive relation of intermediate materials between ideal solid and Newtonian fluid.

It can be seen from the previous analysis that the creep failure process of the mudstone interlayer is divided into three stages, namely, initial creep, steady-state creep, and accelerated creep. The improved model selected in this paper consists of three parts, as shown in Figure 15. The Hooke body represents the instantaneous deformation caused by stress loading, the Abel dashpot represents the initial creep and steady-state creep, and the fractional viscoplastic body composed of the variable coefficient Abel dashpot and the plastic element in parallel represents the nonlinear accelerated creep. The constitutive relation of variable coefficient Abel dashpot can refer to references [36].

The constitutive relation of the improved creep model is expressed as follows ($\sigma \geq \sigma_s$):

$$\varepsilon(t) = \frac{\sigma}{E_0} + \frac{\sigma}{\eta_1^\gamma} \frac{t^\gamma}{\Gamma(\gamma+1)} + \frac{\sigma - \sigma_s}{\eta_2^\gamma} \times t^\gamma \sum_{k=0}^{\infty} \frac{(\alpha t)^k}{\Gamma(k+1+\gamma)}, \tag{6}$$

where E_0 is the elastic modulus, η_1^γ and η_2^γ are the viscosity coefficients, γ is the derivative order, α is the coefficient related to the properties of the mudstone interlayer, and σ_s is the yield stress.

The fractional order model has a simple relational expression, few parameters, and clear physical meaning, while retaining the Abel dashpot and the Abel dashpot with variable coefficient. Since the nonlinear accelerated creep phase of the rock is not present at the beginning, the variable coefficient Abel dashpot is connected in parallel with the plastic element. When the stress exceeds a critical value σ_s, with the increase of stress and the extension of time, it gradually enters the accelerated creep stage. The initial, steady state, and accelerated creep of rock are described with a unified expression, and the simulation of the whole creep process is realized.

4.3. Fitting Analysis and Applicability Test of Fractional Creep Model. Viscoelastic based on fractional derivative theory and viscoelastic-plastic damage creep models is used, and the least squares method is used to fit and analyze the strains under the conditions of $\sigma \geq \sigma_s$. The fitting results are shown in Table 3, and the test data and fitting curves are shown in Figure 16. The Nishihara model is composed of Hooke body, Kelvin body, and ideal viscoplastic body in series, which can fully reflect the elastic-viscoelastic-viscoplastic properties of rocks, and is widely used to describe the creep properties of rock materials. In order to further illustrate the advantages of the model in this paper, the Nishihara model and the model are now used to fit the experimental data at the same time, and the fitting effects of both models are compared. The constitutive relation of the Nishihara model [37] is

$$\varepsilon(t) = \frac{\sigma}{E_0} + \frac{\sigma}{E_1}\left[1 - \exp\left(-\frac{E_1}{\eta_1} t\right)\right] + \frac{\sigma - \sigma_s}{\eta_2} (\sigma \geq \sigma_s). \tag{7}$$

As can be seen from Figure 16, the theoretical curve of the fractional viscoelastic-plastic model agrees well with the experimental curve. It can be seen from Table 3 that the correlation coefficient (R) of the fractional derivative creep model used in this paper is closer to 1 than the correlation coefficient (R) of the Nishihara model, which indicates

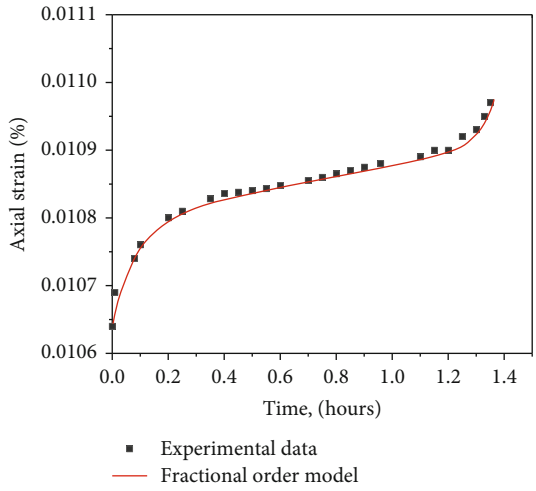

Figure 17: Creep fitting effect of the mudstone interlayer after oil erosion.

that the fractional derivative model fits the experimental data better. By comparing the data of different creep stage, it is found that there is a certain deviation between the fitting curve of the Nishihara model and the data points of the initial creep stage, while the data points of the fitting curve of the fractional viscoelastic-plastic model in this stage are in good agreement with the experimental data. The fitting data points of the fractional derivative creep model is closer to the experimental data, which can better reflect the nonlinear accelerated creep characteristics of salt rock.

After the above analysis, it can be seen that the model in this paper has a good fitting effect on the creep process of the natural mudstone interlayer. The following section will test whether the model is also applicable to mudstone interlayer after oil erosion. In this paper, the model is validated using test data of the mudstone interlayer after oil erosion, and the fitting results are shown in the figure below:

As can be seen from Figure 17, the model developed in this paper is not only suitable for the creep characteristics of natural mudstone interlayer but also can be better deformed by uniaxial compression creep after oil erosion. This shows that the improved model in this paper has a good fit for the uniaxial compression creep characteristics of the mudstone interlayer. Compared with the Nishihara model, the model in this paper can better describe the creep characteristics of the mudstone interlayer and has higher accuracy and applicability.

5. Conclusions

In this study, a graded loading creep test was carried out on the mudstone interlayer taken from the Huai'an salt rock mining area in Jiangsu, and the effect of different stress levels on the creep characteristics of the mudstone interlayer was studied. The experimental results were used to analysis the stress-strain relationship during creep in the mudstone interlayer, to determine the long-term strength of the mudstone interlayer. Finally, the accuracy and applicability of the model are discussed using an improved viscoelastic-plastic graded creep model. The main conclusions are as follows:

(1) When the stress level is low, the axial creep phenomenon of the mudstone interlayer is more significant than that in the lateral direction. With the increase of the stress level, the lateral creep is gradually significant, and the lateral strain becomes more obvious in the approaching failure stage

(2) As the stress level increases, both the transient strain and creep strain of the specimen tend to increase. The change in axial transient strain due to increased internal damage is much more sensitive than the change in transverse transient strain. At high stress levels, the creep phase is more severe in terms of damage accumulation, increasing creep strain and entering the accelerated creep phase, which eventually leads to macroscopic damage

(3) The isochronous strain curve method, the steady-state creep rate inflection point method, and the two-segment power function inflection point method were used to determine the long-term strength of the mudstone interlayer to be approximately 14.97 to 15.34 MPa, which is 60% of the corresponding uniaxial compressive strength. It can be seen that all three long-term strength determination methods are influenced by creep stress levels and loading times

(4) The improved fractional viscoelastic-plastic creep damage model is used to establish the creep constitutive equation under uniaxial compression. This model can describe the three stages of uniaxial compression with a unified expression. The theoretical curve agrees well with the experimental curve and has good applicability to the long-term creep behavior of the mudstone interlayer after oil erosion

Data Availability

The data used to support the findings of this study are available from the corresponding author upon request.

Additional Points

Highlights. ① There are multistage uniaxial creep tests of the typical mudstone interlayer in bedded salt rock energy storage in China: a case study of Huai'an salt mine, Jiangsu Province. ② With AE technology, the damage characteristics from initial loading to stable creep under each stress loading levels are studied. ③ There is a fractional creep constitutive model of argillaceous salt rock considering damage. ④ The applicability and accuracy of the model are tested.

Conflicts of Interest

The authors declare that they have no competing interests.

Authors' Contributions

We confirm that this manuscript has been read and approved by all authors, and that there no other persons who satisfied the criteria for authorship but are not listed. We further confirm that the order of authors listed in the manuscript has been approved by all of us.

Acknowledgments

The authors gratefully acknowledge the financial supports provided by the National Natural Science Foundation of China (Nos. 52022014, 51834003), which are all greatly appreciated.

References

[1] W. Gang, Y. M. Wei, C. Nielsen, L. Xi, and M. B. Mcelroy, "A dynamic programming model of China's strategic petroleum reserve: general strategy and the effect of emergencies," *Energy Economics*, vol. 34, pp. 1234–1243, 2012.

[2] X. B. Zhang, Y. Fan, and Y. M. Wei, "A model based on stochastic dynamic programming for determining China's optimal strategic petroleum reserve policy," *Energy Policy*, vol. 37, no. 11, pp. 4397–4406, 2009.

[3] R. B. Gao, F. Wu, Q. L. Zou, and J. Chen, "Optimal dispatching of wind-PV-mine pumped storage power station: a case study in Lingxin coal mine in Ningxia Province, China," *Energy*, vol. 243, p. 123061, 2022.

[4] R. B. Gao, F. Wu, J. Chen, C. Zhu, and Q. C. He, "Accurate characterization of triaxial deformation and strength properties of salt rock based on logarithmic strain," *Journal of Energy Storage*, vol. 51, article 104484, 2022.

[5] W. Liu, Z. Z. Zhang, J. Chen et al., "Physical simulation of construction and control of two butted-well horizontal cavern energy storage using large molded rock salt specimens," *Energy*, vol. 185, pp. 682–694, 2019.

[6] W. Liu, Z. X. Zhang, J. Y. Fan, D. Y. Jiang, Z. Y. Li, and J. Chen, "Research on gas leakage and collapse in the cavern roof of underground natural gas storage in thinly bedded salt rocks," *Journal of Energy Storage*, vol. 31, article 101669, 2020.

[7] J. Chen, D. Lu, W. Liu et al., "Stability study and optimization design of small-spacing two-well (SSTW) salt caverns for natural gas storages," *Journal of Energy Storage*, vol. 27, article 101131, 2020.

[8] J. Y. Fan, W. Liu, D. Y. Jiang, J. Chen, W. N. Tiedeu, and J. Daemen, "Time interval effect in triaxial discontinuous cyclic compression tests and simulations for the residual stress in rock salt," *Rock Mechanics and Rock Engineering*, vol. 53, no. 9, pp. 4061–4076, 2020.

[9] X. L. Shi, Q. L. Chen, H. L. Ma, Y. P. Li, T. T. Wang, and C. Zhang, "Geomechanical investigation for abandoned salt caverns used for solid waste disposal," *Bulletin of Engineering Geology and the Environment*, vol. 80, no. 2, pp. 1205–1218, 2021.

[10] W. G. Liang, S. G. Xu, Y. S. Zhao, and C. H. Yang, "Experimental study on creep property of rock salt," *Chinese Journal of Rock Mechanics and Engineering*, vol. 25, no. 7, pp. 1386–1390, 2006.

[11] F. Chen, Y. P. Li, C. H. Yang, and C. Zhang, "Experimental study on creep behaviors of rock salt in Yunying salt mine," *Chinese Journal of Rock Mechanics and Engineering*, vol. 25, no. S1, 2006.

[12] W. Liu, J. Chen, D. Y. Jiang et al., "Tightness and suitability evaluation of abandoned salt caverns served as hydrocarbon energies storage under adverse geological conditions (AGC)," *Applied Energy*, vol. 178, pp. 703–720, 2016.

[13] J. Slizowski and L. Lankof, "Salt-mudstones and rock-salt suitabilities for radioactive-waste storage systems: rheological properties," *Applied Energy*, vol. 75, no. 1-2, pp. 137–144, 2003.

[14] Y. P. Li and C. H. Yang, "Three-dimensional expanded Cosserat medium constitutive model for laminated salt rock," *Rock and Soil Mechanics*, vol. 27, pp. 509–513, 2006.

[15] H. W. Zhou, C. P. Wang, B. B. Han, and Z. Q. Duan, "A creep constitutive model for salt rock based on fractional derivatives," *International Journal of Rock Mechanics and Mining Sciences*, vol. 48, no. 1, pp. 116–121, 2011.

[16] C. H. Yang, T. T. Wang, Y. P. Li et al., "Feasibility analysis of using abandoned salt caverns for large-scale underground energy storage in China," *Applied Energy*, vol. 137, pp. 467–481, 2015.

[17] M. M. Tang, Z. Y. Wang, G. S. Ding, and L. N. Ran, "Creep property experiment and constitutive relation of salt-mudstone interlayer," *Journal of China Coal Society*, vol. 35, no. 1, pp. 42–45, 2010.

[18] H. Cheng, X. P. Zhou, X. K. Pan, and F. Berto, "Damage analysis of sandstone during the creep stage under the different levels of uniaxial stress using NMR measurements," *Fatigue& Fracture of Engineering Materials & Stuructures*, vol. 44, no. 3, pp. 719–732, 2021.

[19] Q. Y. Zhang, W. D. Yang, F. Chen, W. G. Li, and J. H. Wang, "Long-term strength and microscopic failure mechanism of hard brittle rocks," *Chinese Journal of Geotechnical Engineering*, vol. 33, no. 12, pp. 1910–1918, 2011.

[20] F. Wu, H. P. Xie, J. F. Liu, Y. Bian, and J. L. Pei, "Experimental study of fractional viscoelastic-plastic creep model," *Chinese Journal of Rock Mechanics and Engineering*, vol. 33, no. 5, pp. 964–970, 2014.

[21] D. S. Wu, L. B. Meng, T. B. Li, and L. Lai, "Study on rheological properties and long-term strength of limestone triaxial high temperature after heat treatment," *Rock and Soil Mechanics*, vol. 37, no. 1, pp. 183–191, 2016.

[22] F. Wu, R. B. Gao, Q. L. Zou, J. Chen, W. Liu, and K. Peng, "Long-term strength determination and nonlinear creep damage constitutive model of salt rock based on multistage creep test: implications for underground natural gas storage in salt cavern," *Energy Science & Engineeing*, vol. 8, no. 5, pp. 1592–1603, 2020.

[23] J. Chen, *Catastrophic Mechanism Induced by Damaged Surrounding Rock and Mitigation Principle during Bedded Salt Cavern Construction Period*, Chongqing University, Chongqing, 2012.

[24] Y. F. Kang, J. Chen, D. Y. Jiang, W. Liu, and F. Wu, "Damage self-healing property of salt rock after brine immersion under different temperatures," *Rock and Soil Mechanics*, vol. 40, no. 2, pp. 187–195, 2019.

[25] P. G. Ranjith, D. Jasinge, S. K. Choi, M. Mehic, and B. Shannon, "The effect of CO_2 saturation on mechanical properties of Australian black coal using acoustic emission," *Fuel*, vol. 89, no. 8, pp. 2110–2117, 2010.

[26] P. G. Ranjith, M. Fourar, S. F. Pong, W. Chian, and A. Haque, "Characterisation of fractured rocks under uniaxial loading states," *Rock and Soil Mechanics*, vol. 41, no. S1, pp. 43–48, 2004.

[27] X. Jiang, K. Qian, X. S. Wang, S. X. Gao, and D. Y. Jiang, "Effect of supercritical CO2 on mechanical properties of sandstone using acoustic emission and NMR," *Rock and Soil Mechanics*, vol. 39, no. 4, pp. 208–214, 2018.

[28] C. N. Zou, G. Y. Zhang, S. Z. Tao, S. Y. Hu, X. D. Li, and J. Z. Li, "Geological features, major discoveries and unconventional petroleum geology in the global petroleum exploration," *Petroleum Exploration and Development*, vol. 37, no. 2, pp. 129–145, 2010.

[29] X. H. Ma, A. L. Jia, J. Tan, and D. B. He, "Tight sand gas development technology and practices in China," *Petroleum Exploration and Development*, vol. 39, no. 5, pp. 611–618, 2012.

[30] M. M. Nezhad, H. Zhu, J. Woody, and Q. Chen, "A simplified multiscale damage model for the transversely isotropic shale rocks under tensile loading," *International Journal of Damage Mechanics*, vol. 25, no. 5, pp. 705–726, 2016.

[31] R. B. Gao, F. Wu, J. Chen, C. Zhu, and C. X. Ji, "Study on creep characteristics and constitutive model of typical argillaceous salt rock in energy storage caverns in China," *Journal of Energy Storage*, vol. 50, article 104248, 2022.

[32] H. W. Zhou, C. P. Wang, Z. Q. Duan, M. Zhang, and J. F. Liu, "`Fractional derivative-based rheological constitutive model of salt rock`," *Scientia Sinica-Physica Mechanica & Astronomica*, vol. 42, no. 3, pp. 310–318, 2012.

[33] D. Xu, S. Y. Wu, R. Zhang, Z. T. Zhang, J. F. Zhou, and J. H. Deng, "Creep characteristics and creep model of deep buried marble at Jinping underground laboratory," *Journal of China Coal Society*, vol. 44, no. 5, pp. 1456–1464, 2019.

[34] H. W. Zhou, D. Liu, G. Lei, D. J. Xue, and Y. Zhao, "The creep-damage model of salt rock based on fractional derivative," *Energies*, vol. 11, no. 9, p. 2349, 2018.

[35] F. Wu, R. B. Gao, J. Liu, and C. B. Li, "New fractional variable-order creep model with short memory," *Applied Mathematics and Computation*, vol. 380, no. 1, article 125278, 2020.

[36] F. Wu, H. Zhang, Q. L. Zou, C. B. Li, J. Chen, and R. B. Gao, "Viscoelastic-plastic damage creep model for salt rock based on fractional derivative theory," *Mechanics of Materials*, vol. 150, no. 6, article 103600, 2020.

[37] Z. Y. Zhu, F. Luo, Y. Z. Zhang, D. J. Zhang, and J. L. He, "A creep model for frozen sand of Qinghai-Tibet based on Nishihara model," *Cold Regions Science and Technology*, vol. 167, no. 11, article 102843, 2019.